CHEMMEDCHEM

CHEMISTRY ENABLING DRUG DISCOVERY

Accepted Article

Title: Rational Design of Efficient Organic Phototherapeutic Agents via Perturbation Theory for Enhancing Anticancer Therapeutics

Authors: Yunjian Xu, Menglong Zhao, Licai Wu, Feiyang Li, Mingdang Li, Mingjuan Xie, Shujuan Liu, Wei Huang, and Qiang Zhao

To be cited as: *ChemMedChem* 10.1002/cmdc.201900302

Link to VoR: http://dx.doi.org/10.1002/cmdc.201900302

A Journal of

ChemPubSoc Europe

WILEY-VCH

www.chemmedchem.org

Rational Design of Efficient Organic Phototherapeutic Agents via Perturbation Theory for Enhancing Anticancer Therapeutics

Yunjian Xu,[a] Menglong Zhao,[a] Licai Wu,[a] Feiyang Li,[a] Mingdang Li,[a] Mingjuan Xie,[a] Shujuan Liu,*[a] Wei Huang*[a,b] and Qiang Zhao*[a]

[a] Y. Xu, Dr. M. Zhao, L. Wu, F. Li, M. Li, Prof. S. Liu, Prof. W. Huang and Prof. Q. Zhao
Key Laboratory for Organic Electronics and Information Displays & Jiangsu Key Laboratory for Biosensors
Institute of Advanced Materials (IAM) Nanjing University of Posts and Telecommunications
Nanjing, 210023 (P. R. China)
E-mail: iamsjliu@njupt.edu.cn
provost@nwpu.edu.cn
iamqzhao@njupt.edu.cn

[b] Prof. W. Huang
Shaanxi Institute of Flexible Electronics (SIFE)
Northwestern Polytechnical University
Xi'an 710072 (P.R. China)

Supporting information for this article is given via a link at the end of the document.

Abstract: The development of efficient phototherapeutic agents (PTA) through rational and specific principles exhibits great significance to the biomedical field. Herein, a facile and rational strategy has been presented to design PTA via perturbation theory. According to the theory, through the rational optimization of donor–acceptor structure, heavy atom number and their functionalization position, which can effectively decrease energy gap between the singlet and triplet states and increase spin–orbit coupling constant, the enhanced intersystem crossing rate for singlet oxygen generation and nonradiative transition for photothermal conversion efficiency can be realized simultaneously. Finally, the efficient PTA have been obtained, which exhibited excellent performance on multimode imaging guided synergetic photodynamic/photothermal therapy. Thus, this study expounds the intrinsic mechanism of organic PTA and guides the rational design of more excellent organic PTA via perturbation theory.

Photo-induced therapy (PT), including photothermal therapy and photodynamic therapy, has attracted extensive research interests owing to its non-invasiveness, highly spatiotemporal resolution and easy manipulation.[1] For PT, it is a key issue to develop highly efficient phototherapeutic agents (PTA) that can effectively kill tumor cells.[2] To date, a large number of PTA based on inorganic materials have been investigated for efficient cancer treatment by utilizing their excellent stability, high singlet oxygen generation and photothermal conversion performance.[3] When compared to inorganic materials, organic PTA possesses many advantages, such as inherent biodegradability, low toxicity and flexible design.[4] Therefore, the development of highly efficient organic PTA is a good alternative approach for PT.

Generally speaking, an excellent organic PTA should exhibit strong near-infrared (NIR) light capture capability, namely intense NIR absorption for singlet oxygen generation, photothermal and other conversion simultaneously.[5] Up to now, cyanine, phthalocyanine, squaric acid, rhodamine and aza-boron-dipyrromethene (aza-BODIPY) derivatives have been used as photosensitizers (PSs) or photothermal agents for efficient anticancer by utilizing heavy atom effects, photoinduced electron transfer (PET) mechanism or combination of various electronic donors and acceptors.[6] Most of these works, however, are based on trial and error discovery. To date, there were only few works about PTA reported following specific design principles.[7] Thereby, a facile and rational design strategy to develop highly efficient organic PTA was necessary.

Herein, we establish a rational strategy to design highly efficient PTA via perturbation theory. According to the theory, the intersystem crossing (ISC) rate constant (k_{ISC}) was shown as below:[8]

$$k_{ISC} \propto \left\langle {}^1\Psi \middle| \hat{H}_{SO} \middle| {}^3\Psi \right\rangle / \exp(\Delta E_{ST}^{2}) \quad (1)$$

where $\left\langle {}^1\Psi \middle| \hat{H}_{SO} \middle| {}^3\Psi \right\rangle$ and ΔE_{ST} were the spin–orbit coupling (SOC) matrix element and the energy gap between the singlet and triplet states, respectively. Namely, large SOC constant and narrow ΔE_{ST} contributed to the enhanced ISC process.[9] Besides, heavy atom effect can effectively increase $\left\langle {}^1\Psi \middle| \hat{H}_{SO} \middle| {}^3\Psi \right\rangle$ for improving k_{ISC} and quench fluorescence for enhancing nonradiative conversion,[10] which help to increase singlet oxygen generation and photothermal conversion performance.

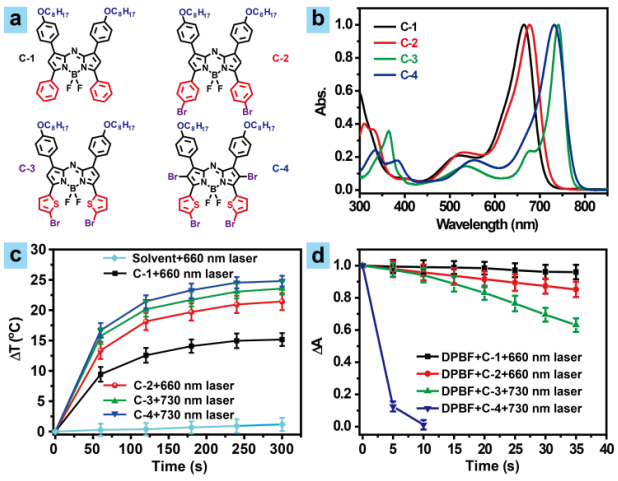

Figure 1. (a) Chemical structures of aza-BODIPY dyes **C-1** – **C-4**. (b) UV-vis absorption spectra of **C-1** – **C-4** in CH_2Cl_2. The absorption intensity has been normalized. (c) Temperature rise of samples in CH_2Cl_2 under irradiation (660 or 730 nm, 0.4 W cm^{-2}) with time. The ambient temperature was 15 °C. (d) The consumption of DPBF in its various mixtures under irradiation (660 or 730 nm, 0.4 W cm^{-2}) with time.

Thus, to validate the above strategy, aza-BODIPY derivatives were chosen as the promising candidates of PTA, owing to their high stability, long-wavelength absorption and easily tunable structure.[11] Noteworthily, substitutes in different positions of aza-BODIPY core exhibited considerable difference on their photophysical properties,[12] which offered a great chance to develop excellent PTA. With above consideration, we have rationally designed and facilely synthesized an aza-BODIPY architecture (**C-4**) with enhanced singlet oxygen generation and photothermal conversion performance via perturbation theory. **C-4** was mainly composed of four parts (**Figure 1a**), including aza-BODIPY core, thienyl rings, bromine atoms and flexible alkyl chain. Thienyl rings with small steric hindrance, as the rich electron donor, were conjugated at position 3 and 5 of electron-deficient aza-BODIPY core to form donor and acceptor (D-A) architecture for small ΔE_{ST} and enhanced NIR absorption,[13] as well as increased ISC process by increasing $\langle {}^1\Psi|\hat{H}_{SO}|{}^3\Psi\rangle$.[14] Bromine atoms were included to further enhance ISC and nonradiative transition process.[15] Flexible alkyl chains were introduced to improve the solubility of rigid aza-BODIPY.[16] For comparison, other three aza-BODIPY dyes (**C-1** – **C-3**, **Figure 1a**) containing different substituents (phenyl rings, brominated phenyl rings or brominated thienyl rings) were also designed and synthesized. The detailed synthetic routes and corresponding chemical structures of as-prepared aza-BODIPY dyes (**C-1** – **C-4**) can be found in Supporting Information. Their structures have been fully characterized by NMR and MALDI-TOF-MS spectra.

C-2 showed the red-shifted and enhanced NIR absorption ($\lambda_{abs.}$ = 677 nm, 95400 L mol^{-1} cm^{-1}) for narrower ΔE_{ST} compared to **C-1** ($\lambda_{abs.}$ = 665 nm, 78600 L mol^{-1} cm^{-1}) in CH_2Cl_2 (**Figure 1b** and **Table S1**), owing to the role of bromine atoms to change the highest occupied molecular orbital of aza-BODIPY structure.[12, 17] **C-3** ($\lambda_{abs.}$ = 741 nm, 167300 L mol^{-1} cm^{-1}) and **C-4** ($\lambda_{abs.}$ = 732 nm, 117800 L mol^{-1} cm^{-1}) exhibited further red-shifted and enhanced NIR absorption for further decreased ΔE_{ST} because of the strong electron donating ability and small steric hindrance of thienyl rings (**Figure 1b** and **Table S1**).[18] The narrower ΔE_{ST} helped to the enhanced k_{ISC} for singlet oxygen generation. The large molar extinction coefficient manifested their strong light capture ability for promising singlet oxygen generation, photothermal and other conversion. **C-1**, **C-2, C-3** and **C-4** also showed sharp NIR emission peaks in the region of 675 – 825 nm, and their maximal emission peaks were at 698 nm, 712 nm, 760 nm and 766 nm, respectively (**Figure S1** and **Table S1**), indicating their potential bioimaging performance in vivo. Their corresponding fluorescence quantum yields were 0.126, 0.049, 0.048 and 0.006 in turn (**Table S1**), indicating that the heavy atom effect could effectively quench fluorescence to increase nonradiative decay for photothermal conversion.

To demonstrate the enhanced photothermal conversion of **C-4** via heavy atom effect, we investigated the photothermal performance of **C-1**, **C-2**, **C-3** and **C-4** by recording their temperature change under a 660 or 730 nm laser irradiation. **C-4**, **C-3**, **C-2** and **C-1** showed the decreased temperature changes as 23.1 °C, 22.6 °C, 18.2 °C and 13.4 °C, respectively (**Figure 1c**), indicating the positive influence of heavy atom effect on photothermal conversion ability of aza-BODIPY core. The introduction of heavy atom (Br or I) was an effective method to increase ISC process for efficient singlet oxygen generation as reported by Eisenberg, Akkaya and their coworkers.[19-24] We then explored the singlet oxygen generation capacity of **C-1**, **C-2**, **C-3** and **C-4** by monitoring the photo-oxidation of 1,3-diphenylisobenzofuran (DPBF) under a 660 nm or 730 nm laser irradiation. The introduction of sulphur and bromine atoms can promote ISC process for enhanced singlet oxygen generation capacity, especially, bromine atoms at 2 and 6 position of aza-BODIPY core led to the best performance (**Figure 1d** and **S2**).

To further validate the positive influence of heavy atom effect to promote photothermal conversion and singlet oxygen generation performance, time-resolved photoluminescence (TRPL) spectra were first measured. Under the same excitation condition, **C-2** (τ = 1.73 ns) and **C-4** (τ = 0.82 ns) displayed the weaker emission and shorter photoluminescence lifetimes than **C-1** (τ = 2.49 ns) and **C-3** (τ = 3.09 ns), respectively (**Figure 2a** and **2b**). **C-3** showed the longer photoluminescence lifetimes than **C-2.** The result was attributed to the effective electron transfer from thienyl rings to aza-BODIPY core caused by the small steric hindrance and excellent electron-rich performance of thienyl rings (**Figure 2a** and **2b**). The above results collectively validated the positive influence of heavy atom effect to enhance photothermal conversion ability. The positive influence of heavy atom effect to enhance singlet oxygen generation performance was then explored by theory calculations. **C-1**, **C-2**, **C-3** and **C-4** presented the increased SOC constants as 0.14, 8.79, 57.81 and 99.16 cm^{-1} (**Figure 2c**), accompanying with a decreased ΔE_{ST} as 1.22, 1.20, 1.11 and 1.10 eV in turn, respectively, suggesting the largest k_{ISC} of **C-4** for the best singlet oxygen generation performance according to the perturbation theory. Noteworthily, the results of theory calculations were well consistent with the experimental data. These principles provided a guidance to develop highly efficient PTA for imaging-guided tumor therapy (**Figure 2d**).

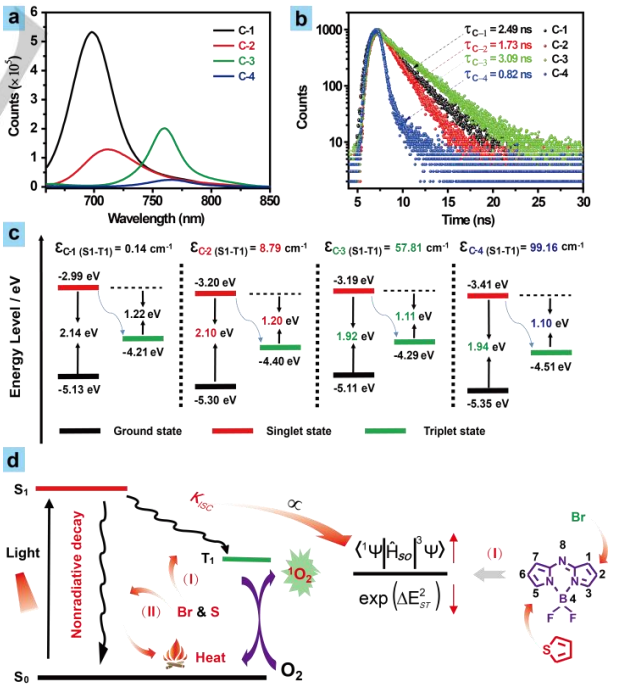

Figure 2. (a) Emission spectra of **C-1**, **C-2**, **C-3** and **C-4** in CH_2Cl_2 (10 μM) (λ = 650 nm). (b) Time-resolved photoluminescence spectra of **C-1**, **C-2**, **C-3** and **C-4** in CH_2Cl_2 (10 μM). (c) Energy level diagrams and SOC coefficients (ε) for **C-1** – **C-4** were obtained by theoretical calculations, respectively. (d) Proposed mechanism for PT enhancement.

C-4 with the best photothermal conversion capacity and singlet oxygen generation performance was used for the biological application in vivo. Water-soluble and biocompatible **C-4** nanoparticles (**C-4 NPs**) with 500 μM were obtained via the relationship of concentration-dependent absorption of **C-4** in CH_2Cl_2 according to previous report (**Figure S3**).[25] They exhibited spherical architecture with hydrodynamic diameter of 91.3 nm (**Figure S4a**) in PBS (pH 7.4), indicating their promising tumor passive targeting capacity by enhanced permeation retentioneffect (EPR) effect.[26] **C-4 NPs** exhibited absorption with a maximal peak and a shoulder peak at 695 nm and 747 nm **(Figure S4b)**, respectively, and dual emission **(Figure S4b)**, which resulted from the aggregation of **C-4** in micelle,[13] suggesting their promising fluorescence imaging (FI) performance. Meanwhile, concentration-dependent PA and FI amplitudes of **C-4 NPs** provided possibility for quantitative analysis of the distribution of **C-4 NPs** (**Figure S5**). The excellent photobleaching, photothermal and RONS (such as H_2O_2 and $ONOO^-$) resistance of **C-4 NPs** was an important inherent property of phototherapeutic agents for tumor imaging and therapy,[27] which has been first confirmed (**Figure S6**). **C-4 NPs** also showed concentration- and laser-power-dependent temperature changes, and continuous generation of singlet oxygen with irradiation time (**Figure S7**), indicating their promising synergistic PDT/PTT performance. They also displayed high photothermal conversion efficiency as 35.9% (**Figure S8**), which was higher than common photothermal agents.[28]

To explore the excellent phototherapeutic performance of **C-4 NPs** in vivo, the in vitro concentration-dependent Hela cells and 3T3 cells viability for **C-4 NPs** was first investigated to evaluate their dark cytotoxicity. The cells still retained a high viability (>83%) even treated with various concentrations of **C-4 NPs** (up to 150 μM) (**Figure 3a**), indicating almost no dark cytotoxicity of **C-4 NPs**. The generation of singlet oxygen in vitro cytotoxicity of **C-4 NPs**. The generation of singlet oxygen in vitro was validated by cell imaging (**Figure 3b**). The laser-power-dependent Hela cells viability was investigated. Hela cells were treated with **C-4 NPs** (15 μM), **C-4 NPs** under hypoxia (oxygen, 5%), **C-4 NPs** plus vitamin C (VC) or saline, respectively. The cell viability showed negative correlations with laser power (**Figure 3c**). Under the same irradiated condition, the cells incubated with **C-4 NPs** plus hypoxia exhibited higher cells viability than those treated by **C-4 NPs**, but lower than those treated by **C-4 NPs** plus VC (**Figure 3c**). The results manifested that photodynamic performance of **C-4 NPs** existed in phototherapy, which acted as an important part even under hypoxia. The fluorescence live/dead cell imaging and flow cytometry experiments also verified the same results (**Figure 3d**, **S9** and **S10**).

Inspired by the concentration-dependent photoacoustic, fluorescence and photothermal properties of **C-4 NPs** in vitro, the EPR effects of **C-4 NPs** were investigated by FI and photoacoustic imaging (PAI). Tumors exhibited the brightest fluorescence signal with high signal-to-noise ratio (SNR) as about 3.0 at 6 h post intravenous injection of **C-4 NPs** (150 μM, 200 μL) (**Figure 4a** and **4c**), suggesting the effective accumulation of **C-4 NPs** in tumors. Meanwhile, the tumors also presented obviously enhanced photoacoustic signal (SNR was about 2.5) compared to those before injection (**Figure 4b** and **4d**). The **C-4 NPs** were mainly

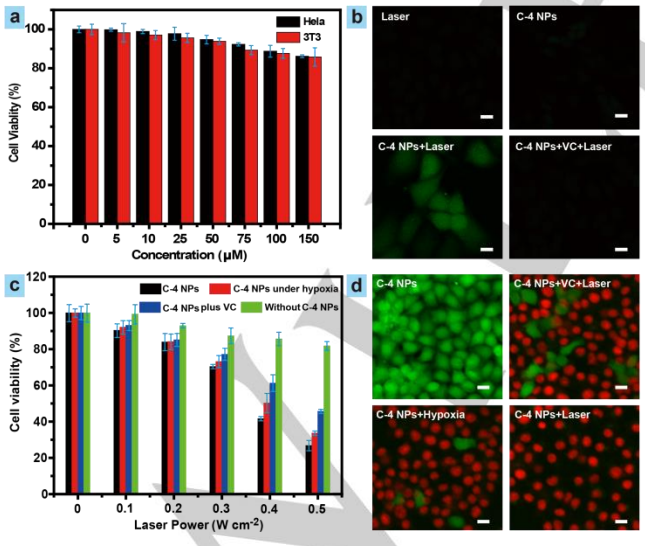

Figure 3. (a) The viability of cells treated with different concentrations of **C-4 NPs**, respectively. (b) Cell imaging for **C-4 NPs** (15 μM)-mediated ROS generation. The scale bar of all images was 20 μm. (c) The viability of cells incubated with **C-4 NPs** (15 μM) or not, and other treatment under various laser irradiation (730 nm, 5 min). (d) The imaging of Hela cells treated with **C-4 NPs** only, **C-4 NPs** + VC + laser, **C-4 NPs** + laser, **C-4 NPs** plus hypoxia, PBS and laser, respectively (15 μM, 730 nm, 0.4 W cm^{-2}, 5 min). All the images share the same scale bar of 20 μm.

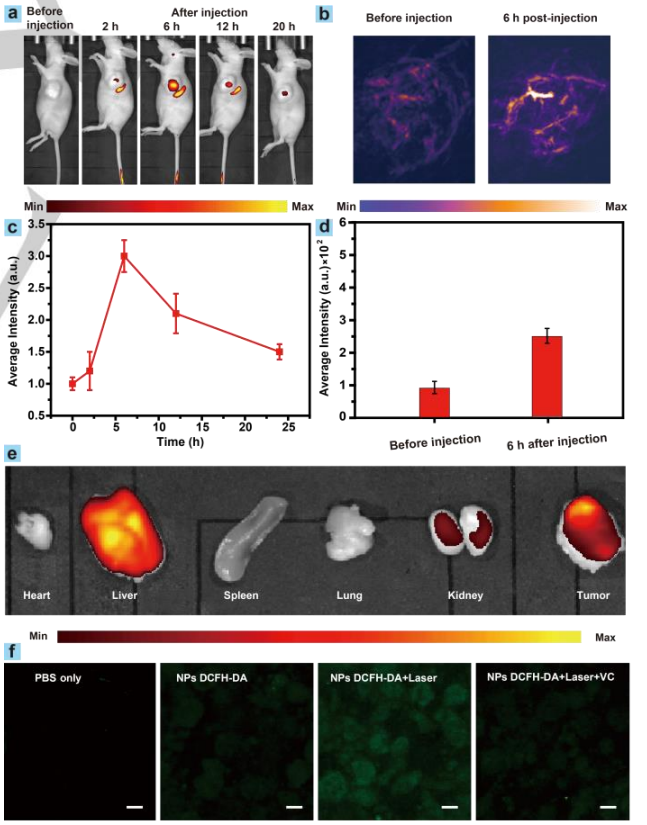

Figure 4. (a) Fluorescence and (b) photoacoustic imaging of mouse before and after injection of **C-4 NPs** (150 μL, 200 μM). (c) and (d) were the average signal intensity of (a) and (b), respectively. (e) **C-4 NPs** distribution in different organs 6 h after its injection. (f) The mice tumor sections imaging after **C-4 NPs** (150 μL, 200 μM) injection or not for 6.5 h. VC acted as singlet oxygen quencher, which was intratumorally injected after **C-4 NPs** (150 μL, 200 μM) injection for 6 h. 0.5 h later, the tumor part was irradiated (730 nm, 0.4 W cm^{-2}, 5 min). The scale bar of all images was 20 μm.

distributed in tumors and livers at 6 h post intravenous injection of them (**Figure 4e**)**,** which could confirm the same results. Finally, the weaker or even negligible FI signal was observed after 20 h (**Figure 4a**), suggesting that **C-4 NPs** in tumor parts could be completely metabolized. Besides, hypoxia in tumors could weaken PDT effect, and singlet oxygen generation in tumor parts was also validated by confocal microscopy images of tumor section mice injected with **C-4 NPs**, suggesting sufficient singlet oxygen generation for PDT in tumor sites during phototherapy (**Figure 4f**).

Rational temperature change was key for highly efficient tumor therapy.[28] The tumor part of mice at 6 h post intravenous injection of **C-4 NPs** in different concentrations was irradiated, respectively, which showed concentration-dependent temperature increase (**Figure 5a**). The tumor temperature was 51.3 °C after 5 min irradiation (**Figure 5a**),[29] manifesting the promising PTT in vivo with **C-4 NPs** at 150 μM.

Inspired by the excellent photothermal and photodynamic performance, and good EPR effect of **C-4 NPs** in vivo, phototherapy of tumor-bearing mice was conducted after intravenous injection of samples for 6.5 h in vivo. The tumor-bearing mice were treated with **C-4 NPs** plus light (PDT+PTT), **C-4 NPs** plus light and VC (PTT), only **C-4 NPs**, only light and only saline, respectively. The tumors in PDT+PTT and PTT groups could be effectively inhibited, and they were removed before the seventh therapy, indicating the excellent phototherapeutic effects. The PDT+PTT group presented slightly better effects than PTT group (**Figure 5b**), due to the fact that the aggravated hypoxic environment weakened the singlet oxygen generation during phototherapy with time. Finally, the removed tumors exhibited no recurrence after 20 d treatment (**Figure 5b**). The tumors sizes in the rest groups presented slightly better effects than PTT group (**Figure 5b**), due to the fact that the aggravated hypoxic environment weakened the singlet oxygen generation during phototherapy with time. The tumors sizes in the rest groups presented obvious growth with sizes about 7 - 10 times of the original value after 20 d treatment (**Figure 5b**). The mice weight in all groups exhibited almost no fluctuation (**Figure 5c**), and the histological hematoxylin and eosin staining showed no obvious pathological discrepancy among all groups in tumors and main organs (**Figure 5d**), suggesting that the only **C-4 NPs** or only laser did almost no harm to mice.

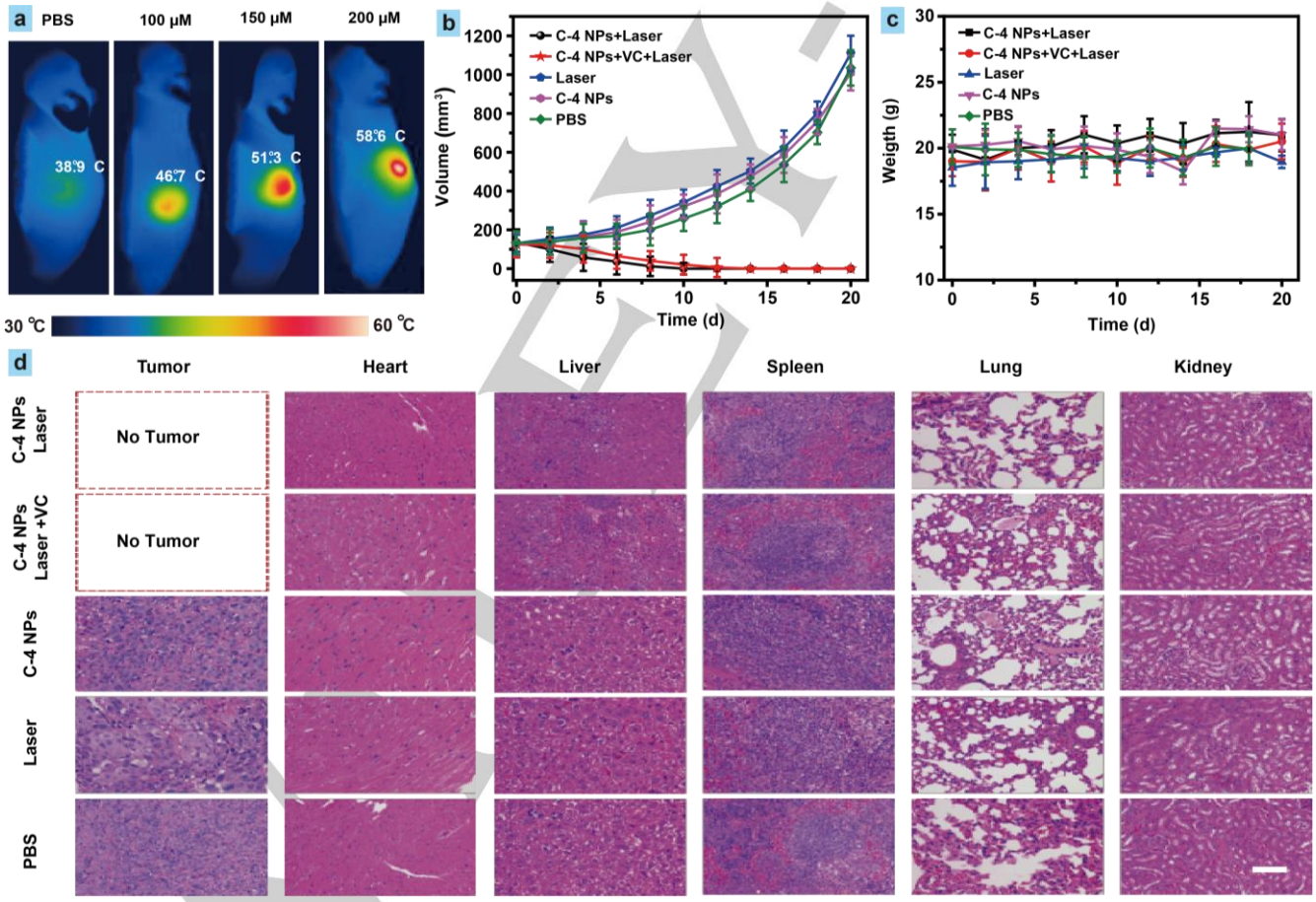

Figure 5. Photothermal therapy in vivo. (a) Photothermal imaging of mice intravenously injected with **C-4 NPs** in different concentrations. (b) The tumor size and (c) body weight of Hela tumor-bearing mice with various treatments during treatments, respectively. (d) H&E staining of tumor and major organs sections obtained from the mice with different treatments. All the images share the same scale bar of 300 μm. Images were taken at 25 °C.

In summary, highly efficient PTA **C-4 NPs** based on aza-BODIPY with D-A structure has been rationally developed via perturbation theory. The systematic investigation of theoretical calculation, fluorescence quantum yield, photothemal conversion efficiency and singlet oxygen generation ability have confirmed that the rational optimization of donor–acceptor structure, heavy atom number and their functionalization position can effectively decrease energy gap between the singlet and triplet states and increase spin–orbit coupling constant, which contributes to the enhanced intersystem crossing rate for singlet oxygen generation and nonradiative transition for photothermal conversion efficiency simultaneously. Noteworthily, water soluble **C-4 NPs** showed concentration-dependent photoacoustic and fluorescent signal, high photothermal conversion efficiency (η = 35.9%) and abundant singlet oxygen generation ability. FI, PAI and PTI of **C-4 NPs** in vivo manifest that **C-4 NPs** can efficiently accumulate in tumor parts via EPR effects. The **C-4 NPs** show efficient therapeutic performance without recurrence when utilized in vivo with mild condition, demonstrating their efficient phototherapeutic performance. This study will offer more interesting exploration on the multifunctional nanotheranostic agents for potential clinical applications.

Experimental Section

*Synthesis of **C-4**:* **C-3** (92 mg, 0.1 mmol) and N-bromosuccinimide (NBS) (100 mg, 0.3 mmol) were dissolved in dry CH_2Cl_2 (10 mL). Then they reacted for 5 h. The final blue solid **C-4** (103 mg, Yield: 95 %) was obtained by recrystallization. ^{1}H NMR (400 MHz, $CDCl_3$) δ(ppm): 7.91 (d, *J* = 4.4 Hz, 2H), 7.80 (d, *J* = 8.8 Hz, 4H), 7.21 (d, *J* = 4.4 Hz, 2H), 6.95 (d, *J* = 8.8 Hz, 4H), 4.02 (t, *J* = 6.8 Hz, 4H), 1.86-1.79 (m, 4H), 1.52 – 1.45 (m, 4H), 1.38 – 1.29 (m, 16H), 0.92-0.88 (m, 6H). ^{13}C NMR (100 MHz, $CDCl_3$) δ(ppm): 160.64, 148.03, 144.68, 142.52, 135.53, 132.51, 131.87, 131.10, 122.87, 121.21, 114.13, 108.82, 68.20, 31.90, 30.15, 29.56, 29.26, 26.09, 22.69, 14.13. ^{19}F NMR (376.5 MHz, $CDCl_3$) δ(ppm): -132.06 (q, 2F). MALDI-TOF-MS m/z: 1080.97.

Animals Model and Tumor Assay: All Hela tumor bearing nude mice were obtained from Nanjing Mergene Life Science Co., Ltd. and used following to the guideline of the Laboratory Animal Center of Nanjing Mergene Life Science Co., Ltd. When the tumor volume of Hela tumor bearing nude mice was about 100 - 200 mm^3, the Hela tumor-bearing mice were randomly divided into five groups. They were treated with I) **C-4 NPs** (200 μL, 150 μM) + laser irradiation (730 nm, 0.4 W cm^{-2}, 5 min), II) **C-4 NPs** + VC (25.0 μmol kg^{-1}) + laser irradiation, III) PBS + laser irradiation, IV) **C-4 NPs** only, V) PBS only, respectively. After the mice were intravenously injected with **C-4 NPs** for 6 h, the VC was intratumorly injected into the tumor. 0.5 h later, mice were irradiated. The size of tumor and the body weight of Hela tumor bearing nude mice were recorded every two days for 20 days. At day 20, the major organs and tumors were acquired for hematoxylin-eosin staining.

The detailed synthetic route of the all compounds and experimental conditions can be acquired in the Supporting Information.

Acknowledgements

The authors acknowledge financial support from the National Funds for Distinguished Young Scientists (61825503), the National Program for Support of Top-Notch Young Professionals, the Priority Academic Program Development of Jiangsu Higher Education Institutions (YX03001), National Natural Science Foundation of China (51473078 and 21671108), National Program for Support of Top-Notch Young Professionals, Scientific and Technological Innovation Teams of Colleges and Universities in Jiangsu Province (TJ215006).

Conflict of interest

The authors declare no conflict of interest.

Keywords: phototherapeutic agent • aza-BODIPY • heavy atom effect • perturbation theory • multimode imaging

References:

[1] C. A. Choi, J. E. Lee, Z. A. I. Mazrad, Y. K. Kim, I. In, J. H. Jeong, S. Y. Park, *ChemMedChem* **2018**, *13*, 1459-1468.
[2] W. Zhao, A. Li, A. Zhang, Y. Zheng, J. Liu, *ChemMedChem* **2018**, *13*, 2134-2149.
[3] X. Han, J. Huang, H. Lin, Z. Wang, P. Li, Y. Chen, *Adv. Healthcare Mater.* **2018**, *7*, 1701394.
[4] Y. Tian, R. Guo, Y. Wang, W. Yang, *Adv. Healthcare Mater.* **2016**, *5*, 3099.
[5] H. S. Jung, P. Verwilst, A. Sharma, J. Shin, J. L. Sessler, J. S. Kim, *Chem. Soc. Rev.* **2018**, *47*, 2280-2297.
[6] M. Li, T. Xiong, J. Du, R. Tian, M. Xiao, L. Guo, S. Long, J. Fan, W. Sun, K. Shao, X. Song, J. W. Foley, X. Peng, *J. Am. Chem. Soc.* **2019**, *141*, 2695-2702.
[7] Y. Xu, M. Zhao, L. Zou, L. Wu, M. Xie, T. Yang, S. Liu, Wei Huang, Q. Zhao, *ACS Appl. Mater. Interfaces* **2018**, *10*, 44324-44335.
[8] S. Yeganeh, M. R. Wasielewski, M. A. Ratner, *J. Am. Chem. Soc.* **2009**, *131*, 2268-2273.
[9] S. Xu, Y. Yuan, X. Cai, C. Zhang, F. Hu, J. Liang, G. Zhang, D. Zhang, B. Liu, *Chem. Sci.* **2015**, *6*, 5824-5830.
[10] J. Zhao, W. Wu, J. Sun, S. Guo, *Chem. Soc. Rev.* **2013**, *42*, 5323-5351.
[11] Y. Ge, D. F. O'Shea, *Chem. Soc. Rev.* **2016**, *45*, 3846-3864.
[12] H. Lu, J. Mack, Y. Yang, Z. Shen, *Chem. Soc. Rev.* **2014**, *43*, 4778-4823.
[13] Q. Tang, W. Si, C. Huang, K. Ding, W. Huang, P. Chen, Q. Zhang, X. Dong, *J. Mater. Chem. B* **2017**, *5*, 1566-1573.
[14] Y. Cai, P. Liang, Q. Tang, X. Yang, W. Si, W. Huang, Q. Zhang, X. Dong, *ACS Nano* **2017**, *11*, 1054-1063.
[15] J. Tian, J. Zhou, Z. Shen, L. Ding, J. Yu, H. Ju, *Chem. Sci.* **2015**, *6*, 5969-5977.
[16] M. Zhao, Y. Xu, M. Xie, L. Zou, Z. Wang, S. Liu, Q. Zhao, *Adv. Healthcare Mater.* **2018**, *7*, 1800606.
[17] A. Gorman, J. Killoran, C. O'Shea, T. Kenna, W. M. Gallagher, D. F. O'Shea, *J. Am. Chem. Soc.* **2004**, *126*, 10619-10631.
[18] J. Qi, Y. Fang, R. T. K. Kwok, X. Zhang, X. Hu, J. W. Y. Lam, D. Ding, B. Tang, *ACS Nano* **2017**, *11*, 7177-7188.
[19] K. M. Farrell, M. M. Brister, M. Pittelkow, T. I. Sølling, C. E. Crespo-Hernández, *J. Am. Chem. Soc.* **2018**, *140*, 11214-11218.
[20] B. Kilic, Nisa Yesilgul, V. Polat, Z. Gercek, E. U. Akkaya, *Tetrahedron Lett.* **2016**, *57*, 1317-1320.
[21] R. P. Sabatini, T. M. McCormick, T. Lazarides, K. C. W, R. Eisenberg, D. W. McCamant, *J. Phys. Chem. Lett.* **2011**, *2*, 223-227.
[22] S. Duman, Y. Cakmak, S. Kolemen, E. U. Akkaya, Y. Dede, *J. Org. Chem.* **2012**, *77*, 4516-4527.
[23] Y. Cakmak, S. Kolemen, S. Duman, Y. Dede, Y. Dolen, B. Kilic, Z. Kostereli, L. T. Yildirim, A. L. Dogan, D. Guc, E. U. Akkaya, *Angew. Chem. Int. Ed.* **2011**, *50*, 11937-11941.
[24] Y. Cakmak, T. Nalbantoglu, T. Durgut, E. U. Akkay, *Tetrahedron Lett.* **2014**, *55*, 538-540.
[25] W. Hu, H. Ma, B. Hou, H. Zhao, Y. Ji, R. Jiang, X. Hu, X. Lu, L. Zhang, Y. Tang, Q. Fan, W. Huang, *ACS Appl. Mater. Interfaces* **2016**, *8*, 12039-12047.
[26] Y. Dai, C. Xu, X. Sun, X. Chen, *Chem. Soc. Rev.* **2017**, *46*, 3830-3852.

[27] J. Weber, P. C. Beard, S. E. Bohndiek, *Nat. Methods* **2016**, *13*, 639-650.
[28] X. Song, Q. Chen, Z. Liu, *Nano Res.* **2015**, *8*, 340-354.
[29] T. Yang, L. Liu, Y. Deng, Z. Guo, G. Zhang, Z. Ge, H. Ke, H. Chen, *Adv. Mater.* **2017**, *29*, 1700487.

Entry for the Table of Contents

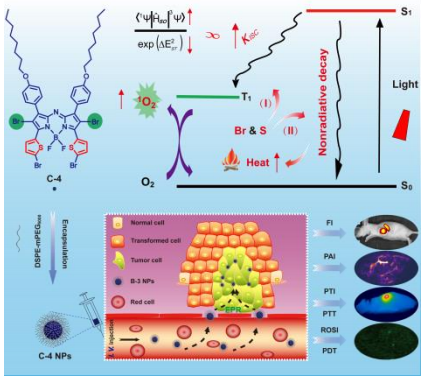

The aza-BODIPY (**C-4**) based phototherapeutic agent (PTA) with enhanced anticancer efficacy has been rationally designed via perturbation theory. According to the theory, **C-4** with improved singlet oxygen generation and photothermal conversion efficiency simultaneously has been obtained through the rational optimization of structure. Finally, the PTA successfully cures tumors without recurrence under multimode imaging guided phototherapy.